Rational Engineering of an Improved Genetically Encoded pH Sensor Based on Superecliptic pHluorin

Yi Shen, Yurong Wen, Silvia Sposini, Anjali Amrapali Vishwanath, Ahmed Abdelfattah, Eric Schreiter, M. Joanne Lemieux, Jaime de Juan-Sanz, David Perrais, Robert Campbell

ACS SENSORS

pubs.acs.org/acssensors

Article

Rational Engineering of an Improved Genetically Encoded pH Sensor Based on Superecliptic pHluorin

Yi Shen,* Yurong Wen, Silvia Sposini, Anjali Amrapali Vishwanath, Ahmed S. Abdelfattah, Eric R. Schreiter, M. Joanne Lemieux, Jaime de Juan-Sanz, David Perrais, and Robert E. Campbell*

Cite This: https://doi.org/10.1021/acssensors.3c00484

Read Online

ACCESS | Metrics & More | Article Recommendations | Supporting Information

ABSTRACT: Genetically encoded pH sensors based on fluorescent proteins are valuable tools for the imaging of cellular events that are associated with pH changes, such as exocytosis and endocytosis. Superecliptic pHluorin (SEP) is a pH-sensitive green fluorescent protein (GFP) variant widely used for such applications. Here, we report the rational design, development, structure, and applications of Lime, an improved SEP variant with higher fluorescence brightness and greater pH sensitivity. The X-ray crystal structure of Lime supports the mechanistic rationale that guided the introduction of beneficial mutations. Lime provides substantial improvements relative to SEP for imaging of endocytosis and exocytosis. Furthermore, Lime and its variants are advantageous for a broader range of applications including the detection of synaptic release and neuronal voltage changes.

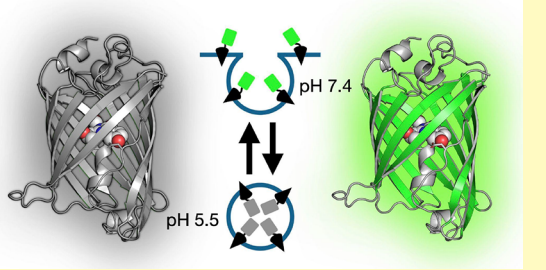

KEYWORDS: *pHluorin, fluorescent proteins, genetically encoded sensors*

Genetically encoded sensors based on fluorescent proteins (FPs) are essential tools for studying molecular and cellular physiology.[1,2] Over the past two decades, an expanded toolkit of FP-based sensors has been engineered to monitor numerous biochemical parameters including the Ca^{2+} concentration, membrane potential, neurotransmitter dynamics, and pH.[3,4] pH changes are tightly associated with cellular processes such as endocytosis and exocytosis. Using the example of synaptic transmission, the lumen of synaptic vesicles is typically acidified to pH ∼5.5 by the proton pump activity of vacuolar-type ATPase. Upon fusion of a synaptic vesicle to the plasma membrane, the contents of the vesicle are exposed to the neutral pH (∼7.0 to 7.5) of the extracellular environment.[5] This substantial change in pH allows the process of exocytosis to be visualized using a genetically encoded pH sensor fused with a vesicular membrane-associated protein.[6,7] Monitoring of endocytosis and exocytosis has provided valuable insights that have helped to elucidate the fundamental biology of neurotransmission and have aided investigations of the underlying mechanism of various neurological diseases.[8−11]

Genetically encoded pH sensors are FPs that demonstrate pH-dependent fluorescence spectrum or intensity change within the physiologically relevant pH range.[6,12−17] Most naturally occurring FPs exhibit pH-dependent fluorescence changes, but some are much more sensitive in the physiological range than others. For example, the wild-type *Aequorea victoria* green fluorescent protein (GFP) chromophore exists in a pH-dependent equilibrium between protonated and deprotonated states, which absorb maximally near 400 and 488 nm, respectively.

A pH-sensitive GFP variant, ecliptic pHluorin, was engineered to exhibit dim fluorescence at pH 5.5 when excited at 488 nm while becoming fluorescent at higher pH values, with an apparent pK_a (the pH value at which the fluorescence intensity is 50% of maximal) of 7.1. Fusion of ecliptic pHluorin to VAMP2 produced synapto-pHluorin, which enabled the visualization of synaptic vesicle release and neurotransmission.[6] Incorporating mutations from enhanced GFP (EGFP) led to superecliptic pHluorin (SEP) with an apparent pK_a of 7.2. SEP is nearly nonfluorescent at pH 5.5 but brightly green fluorescent at pH 7.4. An optimal pK_a and low background fluorescence in the protonated state make SEP a nearly ideal tool for the imaging of exocytosis and endocytosis in living cells.[12] Vesicular membrane proteins fused with SEP have been extensively used to detect the exocytosis of synaptic vesicles, secretory vesicles, and recycling endosomes.[8,18,19] SEP has also been used to detect the formation of clathrin-coated vesicles (CCVs) using the pulsed pH (ppH) protocol, which reveals the location of receptors that have been newly internalized with high temporal accuracy.[20,21] A SEP variant, SEP-D (SEP-A227D), serves as the fluorophore of the genetically encoded fluorescent protein voltage sensor ArcLight, which is a fusion

Received: March 14, 2023
Accepted: July 6, 2023

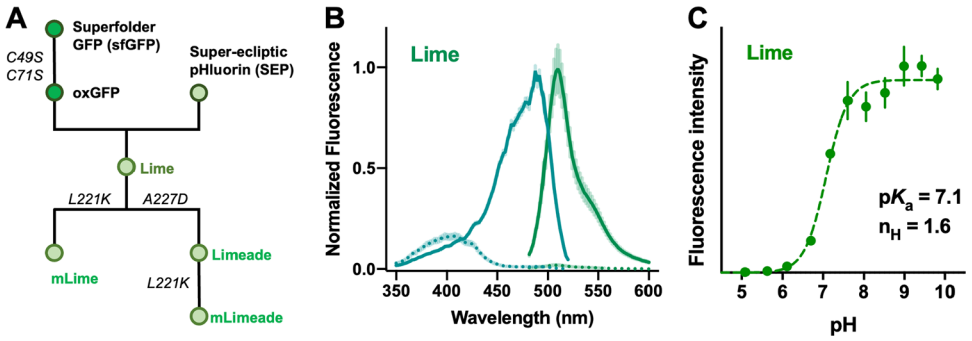

Figure 1. Rational engineering and *in vitro* characterization of Lime. (A) Design and genealogy of Lime and its variants. (B) Fluorescence spectrum of Lime at pH 5.5 (dotted lines) and pH 7.5 (solid lines). (C) pH titration curves of Lime.

Table 1. *In Vitro* Characterization of GFP-Based pH-Sensitive FPs

	extinction coefficient (EC, M^{-1} cm^{-1})	quantum yield (QY)	molecular brightness (EC × QY/1000)	absorption maxima (nm)	excitation maxima (nm)	emission maxima (nm)	pK_a	n_H	fold change (pH 5.6 to 7.2)
EGFP	57,000	0.60	34	488	488	509	5.5	1.0	N.D.[a]
SEP	37,000	0.80	30	490	488	511	7.0	1.7	66 ± 6
SEP-D	31,000	0.80	25	490	488	511	7.2	1.3	70 ± 1
Lime	45,000	0.77	35	483	488	510	7.1	1.6	82 ± 9
mLime	36,000	0.72	26	483	488	509	7.1	1.6	86 ± 2
Limeade	31,000	0.72	22	483	488	509	7.1	1.5	99 ± 1
mLimeade	29,000	0.77	22	483	488	509	7.1	1.5	98 ± 1

[a]N.D., not determined.

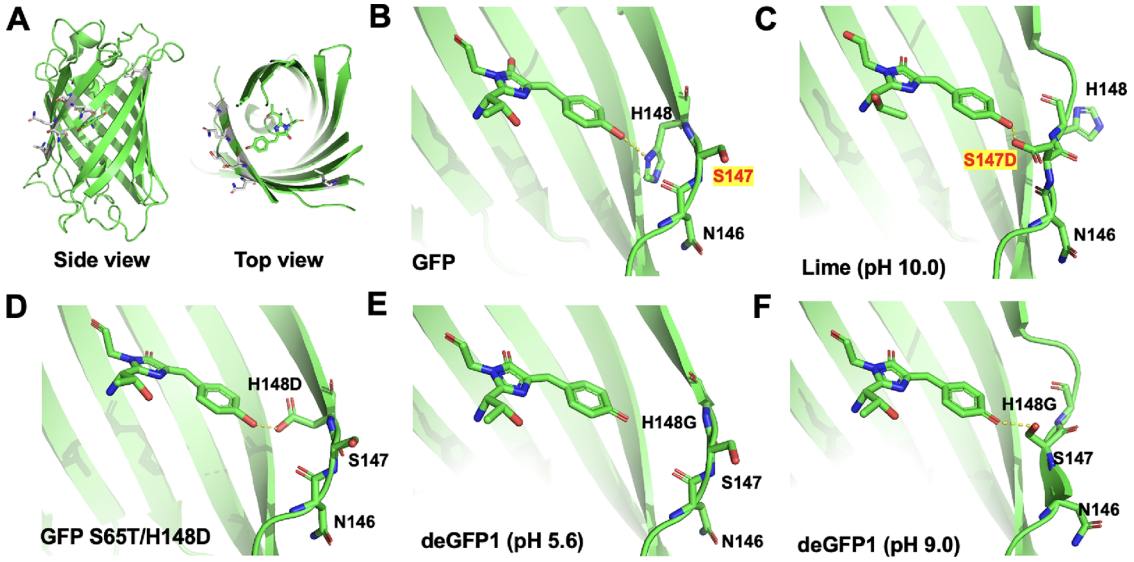

Figure 2. Structural analysis of Lime. (A) SEP mutation positions (from EGFP) are mapped on the structure (left: side view; right: top view) of GFP (PDB 1EMA). The chromophore is shown in green sticks, and mutated residues are shown in gray sticks. (B) In GFP, the side chain of residue S147 points outward from the β-barrel structure. (C) In Lime, the side chain of residue S147D points inward and directly interacts with the chromophore. (D) In the pH-sensitive GFP S65T/H148D variant (PDB 2DUF), H148D is pointing inward and directly interacts with the chromophore. Conformations of residue S147 and H148G in deGFP1 at pH 5.6 (E) (PDB 1JBY) and pH 9.0 (F) (PDB 1JBZ).

of the voltage-sensing domain from *Ciona intestinalis* voltage-sensitive phosphatase to SEP-A227D.[22]

Although widely used, SEP has a few shortcomings such as relatively low brightness and suboptimal trafficking, which limits its utilities in some applications.[10,23−25] Here, we report the design and characterization of Lime, a rationally engineered SEP variant with higher fluorescence brightness and improved performance. Lime takes advantage of the high brightness and expression of sfGFP[26] and is cysteine-free for potentially better compatibility with membrane protein fusion.[27] We determined the X-ray crystal structure of Lime to provide molecular insight into its pH sensitivity. We demonstrated the utility of Lime by imaging endocytosis and exocytosis in cultured cell lines and neuronal activities in dissociated neurons.

RESULTS AND DISCUSSION

Rational Engineering and *In Vitro* Characterization of Lime. Our approach to rationally improving SEP was to incorporate mutations from previously reported GFP variants

https://doi.org/10.1021/acssensors.3c00484
ACS Sens. XXXX, XXX, XXX−XXX

Table 2. *In Vitro* Characterization of EGFP- and mClover3-S147D Mutants

	extinction coefficient (EC, M^{-1} cm^{-1})	quantum yield (QY)	molecular brightness (EC × QY, ×1000)	absorption maxima (nm)	excitation maxima (nm)	emission maxima (nm)	pK_a	n_H	fold change (pH 5.6 to 7.2)
EGFP-S147D	32,000	0.53	17	488	488	509	7.0	1.4	43 ± 2
mClover3-S147D	45,000	0.61	27	507	508	518	7.3	1.0	67 ± 2

with better characteristics. To improve the brightness and expression of SEP, we changed the GFP scaffold from EGFP to superfolder GFP (sfGFP).[26] To make the new variants compatible with oxidative environments such as those within the endoplasmic reticulum (ER) and Golgi, we engineered cysteine-free SEP variants, as previously described for the moxFPs.[27,28] Based on the two aforementioned rationales, we designed the second-generation SEP by incorporating the sfGFP scaffold and eliminating cysteine residues. We synthesized the DNA encoding this designed construct and named it Lime (Figure 1 and Figure S1). Starting from Lime, we further introduced the most effective GFP monomerizing mutation L221K[29] and the key mutation A227D in ArcLight for potential enhancement of pH sensitivity and the ability to be incorporated into genetically encoded voltage indicators (GEVIs).[22] These efforts resulted in three more variants: mLime (Lime-L221K), Limeade (Lime-A227D), and mLimeade (Lime-L221K/A227D) (Figure 1A).

To determine the *in vitro* properties of these new variants, we purified Lime, mLime, Limeade, and mLimeade, together with EGFP, SEP, and SEP-D (SEP-A227D from Arclight) and measured the spectral profile (i.e., absorption maxima, excitation maximum (λ_{ex}), and emission maximum (λ_{em})), photophysical properties (i.e., extinction coefficient (EC) and quantum yield (QY)), and pH sensitivity (i.e., apparent pK_a, apparent Hill coefficients n_H, and fluorescence intensity fold change over pH 5.6 to pH 7.2). At pH 7.5, Lime had λ_{ex} = 488 nm and λ_{em} = 510 nm, while at pH 5.5, the λ_{ex} shifted to 400 nm, and the green fluorescence emission is mostly quenched when excited at 488 nm (Figure 1B). Based on the fluorescence vs pH response curve, Lime exhibited a pK_a of 7.1 and an n_H of 1.6 (Figure 1C). Among all the newly designed variants, Lime exhibited a higher brightness (EC × QY/1000) compared to SEP (35 vs 30, pH 7.9), and it also had a larger fluorescence change (82-fold vs 66-fold) over the physiological pH range (5.6 to 7.2) (Table 1).

Structural and Mutational Analysis. During our initial examination of mutations in SEP, we realized that none of the six mutations of SEP relative to EGFP (S147D/N149Q/T161I/S202F/Q204T/A206T) directly interact with the chromophore based on the structure of GFP (PDB 1EMA, Figure 2A). Of the six mutations, five of them (S147D/N149Q/S202F/Q204T/A206T) are located outside the β-barrel structure, and the other mutation T161I resides on the 8th strand pointing inside of the β-barrel, yet distant from the chromophore. This led us to speculate about the mechanism by which these mutations might modulate the chromophore pK_a from 5.5 (EGFP) to 7.0 (SEP) (Table 1). A previous study suggested a key role for the S147D mutation in shifting the pK_a, but no detailed explanation at the molecular level was provided.[30] To pinpoint the molecular basis of this pK_a shift, we solved the crystal structure of Lime (Table S1). Compared to GFP (PDB 1EMA), which harbors S147 with its side chain directed outward from the β-barrel structure (Figure 2B),[31] the crystal structure of Lime at pH 10.0 revealed that the S147D mutation had induced a significant rearrangement. The side chain of S147D has become inward-facing and is directly interacting with the chromophore, which is certain to be influencing the pK_a of the chromophore (Figure 2C). The direct interaction of the side chain of an aspartic acid with the GFP chromophore has been reported previously in GFP S65T/H148D. In this variant, H148D was found to interact with the chromophore via hydrogen bonding and resulted in an elevated pK_a value of 7.9 (Figure 2D).[32] The conformational rearrangement of the residue at position 147 has also been observed in deGFP1 (S65T/H148G/T203C). In this variant, the side chain of S147 is outward-facing at pH 5.6 but has flipped to inward-facing at pH 9.0 (Figure 2E,F).[33]

To examine possible structure differences at different pH values, we solved structures of Lime at a lower pH of 6.0. Superimposition of the two structures at pH 10 and 6 revealed no major structural rearrangements, with the side chain of S147D pointing inside the FP barrel at both the high and low pH values (Figure S2A). However, the superimposition revealed two relatively subtle structural differences (Figure S2B). First, the chromophore in the higher pH structure adopts a more planar conformation compared to the lower pH structure. The two dihedral angles indicating the chromophore planarity are 8.7 and −5.6° in the pH 10 state, compared with 19.9 and −15.0° in the pH 6 state (Figure S2C,D). Second, the carboxylate group on the S147D side chain in the high pH structure sits closer to the chromophore (distance of 2.7 Å) than in the low pH structure (distance of 3.2 Å) (Figure S2C,D). These conformational changes in the chromophore and its proximity to the S147D side chain are likely associated with the large fluorescence change between high and low pH states.

To further confirm the key role of S147D mutation in pK_a modulation, we introduced this single mutation into GFP variants, EGFP (pK_a of 5.5)[34] and mClover3 (pK_a of 6.5).[35] The pH titrations of EGFP-S147D, and mClover3-S147D both revealed a significant increase in apparent pK_a values to 7.0 and 7.3, respectively. Thus, the S147D mutation effectively makes EGFP and mClover3 into pH-sensitive GFPs similar to SEP and Lime (Table 2), confirming its ability to modulate the pH sensitivity of GFP variants. It remains to be determined if a similar mutation at the aligned position of FPs from organisms other than *Aequorea* (e.g., W138 of mNeonGreen)[36] could have a similar influence on pK_a.

Comparison of Lime and SEP for Imaging Endocytosis and Exocytosis. We next tested the performance of Lime in live-cell imaging and compared it with SEP. The transferrin receptor (TfR) fused to a pH-sensitive GFP (e.g., TfR-SEP) has been widely used for the detection of single endocytosis and exocytosis events in cultured cells.[15,18,20,21,37] We first imaged and quantified endocytic events in the BSC-1 cell line using the pulsed-pH protocol with time-lapse total internal reflection fluorescence (TIRF) imaging at 0.5 Hz. We

https://doi.org/10.1021/acssensors.3c00484
ACS Sens. XXXX, XXX, XXX−XXX

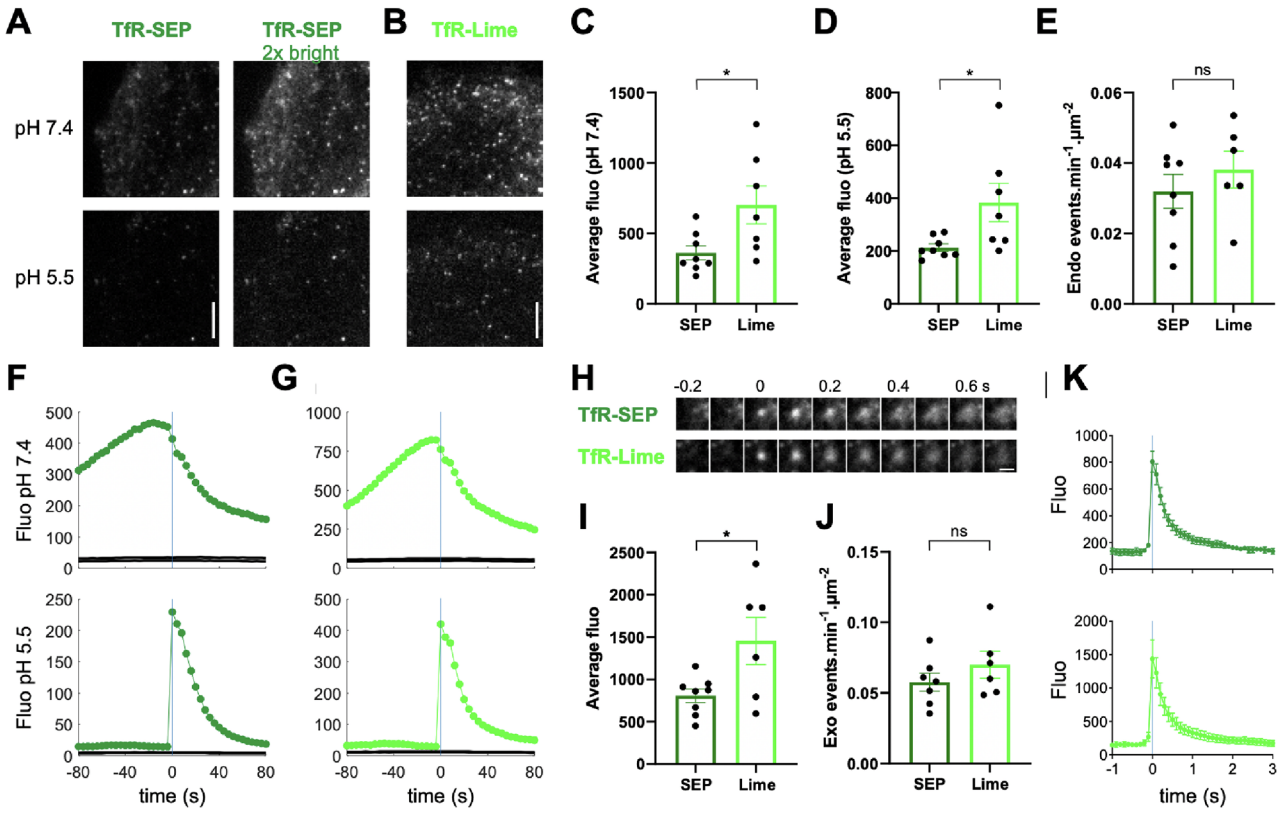

Figure 3. Imaging endocytosis and exocytosis with TfR-Lime. (A,B) Fluorescence images of TfR-SEP (A) and TfR-Lime (B) expressing cells at pH 7.4 and 2 s later at pH 5.5. Scale bar, 5 μm. Fluorescence images of TfR-Lime expressing cells at pH 7.4 and 2 s later at pH 5.5. Scale bar, 5 μm. (C,D) Average fluorescence at the time of scission with TfR-SEP or TfR-Lime at pH 7.4 (C) or pH 5.5 (D) (unpaired *t*-test, $p = 0.027$ and 0.029, respectively). (E) Frequency of detected endocytic events (unpaired *t*-test, $p = 0.404$). (F,G) Average fluorescence time course of endocytosis events reported by TfR-SEP ((F) 3712 events, 8 cells) and TfR-Lime ((G) 4269 events, 7 cells). Black lines represent 95% confidence intervals for randomized events to determine the level of enrichment at sites of scission. (H) Examples of exocytosis events in consecutive frames for cells transfected with TfR-SEP (top) and TfR-Lime (bottom). Scale bar, 1 μm. (I) Average fluorescence at the time of exocytosis for events with TfR-SEP and TfR-Lime (unpaired *t*-test, $p = 0.027$). (J) Frequency of detected exocytic events (unpaired *t*-test, $p = 0.297$). (K) Average fluorescence time course of exocytosis events reported by TfR-SEP (528 events, 8 cells) and TfR-Lime (721 events, 6 cells), aligned to the time of detection (time 0).

used a previously developed algorithm for the determination of the scission events.[20,21] Cells expressing TfR-Lime had brighter fluorescence than the ones expressing TfR-SEP under identical imaging conditions. A Western blot analysis revealed that the amounts of TfR-SEP and TfR-Lime in cells were not significantly different (Figure S3). A two-fold increase in exposure time was required to obtain images of TfR-SEP with intensities that were comparable to TfR-Lime (Figure 3A,B).

Quantitative analysis of the average fluorescence intensity at the time of scission revealed that TfR-Lime offers approximately a two-fold improvement in terms of the fluorescence brightness over TfR-SEP, at both pH = 5.5 and pH = 7.4 (Figure 3C,D). For reasons that remain unclear, the fluorescence intensities for TfR-Lime endocytic events are more variable than for TfR-SEP endocytic events. Both TfR-SEP and TfR-Lime reported similar frequencies of events detected (Figure 3E), confirming that most endocytic events can be detected with both reporter proteins.[37] The average fluorescence time course of endocytosis of TfR-SEP and TfR-Lime reflected similar kinetics, yet again with a substantially higher fluorescence intensity for TfR-Lime (Figure 3F,G). We next imaged exocytic events using continuous TIRF microscopy imaging at 10 Hz (Figure 3H). An exocytotic event manifests as sudden bursts of fluorescence due to the change in pH experienced by the TfR construct followed by dissipation of fluorescence as the TfR construct diffuses away from the exocytosis site, as previously described.[18,38] In agreement with our results for endocytosis, cells expressing TfR-Lime exhibited a significantly higher fluorescence amplitude than TfR-SEP (Figure 3I), yet still reported comparable event frequencies, and had similar fluorescence decay kinetics at sites of exocytosis events, which reflects the rate of protein diffusion away from the fusion site (Figure 3J,K). Overall, our results indicated that Lime has clear advantages over SEP as a useful reporter for TfR exocytosis and endocytic vesicle detection.

Imaging Neuronal Activities with Lime and Its Variants. To evaluate the performance of Lime for imaging neuronal activity, we first attempted to image synaptic vesicle release using synaptophysin-Lime. Lime was incorporated into the intravesicular loop region of vesicle protein synaptophysin.[39] Synaptophysin-Lime expressed in dissociated neurons exhibited well-localized fluorescence at the synapse with low background fluorescence (Figure 4A). Under electric stimulation to evoke action potentials (APs), synaptophysin-Lime responded with a fluorescence change $\Delta F/F_0$ of 19.0 ± 2.9% increase upon 10 stimuli by a field electrode at 10 Hz (Figure 4B, C). Synaptophysin-SEP exhibited a change of 22.6 ± 2.4% under the same conditions. Synaptophysin-Lime also exhibited

https://doi.org/10.1021/acssensors.3c00484
ACS Sens. XXXX, XXX, XXX−XXX

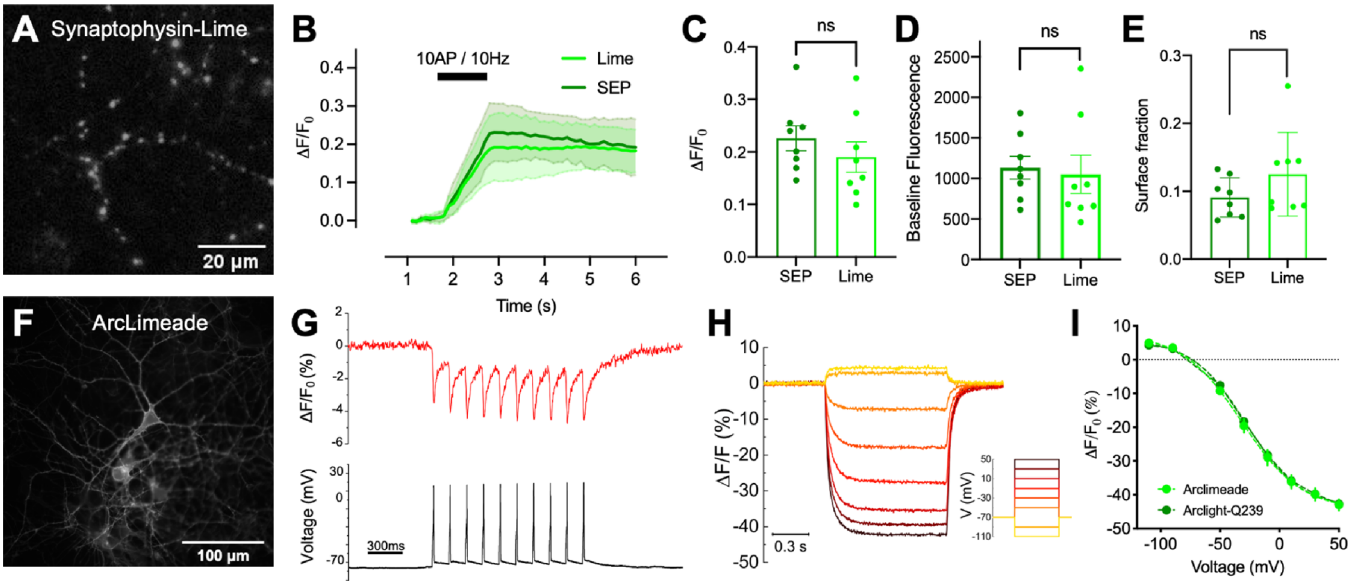

Figure 4. Imaging neuronal activities with synaptophysin-Lime and ArcLimeade. (A) Representative image of neurons expressing synaptophysin-Lime. (B) Synaptophysin-Lime response time course under stimulation of 10 action potentials (AP) at 10 Hz (n = 8). Comparison between synaptophysin-Lime and synaptophysin-SEP in terms of fluorescence change upon 10 stimuli by the field electrode at 10 Hz (C), baseline fluorescence (D), and surface fractions (E). (F) Representative image of neurons expressing ArcLimeade. (G) Simultaneous fluorescence imaging (top) and whole-cell patch-clamp membrane voltage measurements (bottom) from cultured neurons expressing ArcLimeade. (H) Representative fluorescence changes of ArcLimeade to voltage steps from −110 to 50 mV, normalized to the fluorescence at −70 mV. (I) Fluorescence change vs membrane voltage (F–V) curve for ArcLimeade and ArcLight-Q239.

comparable performance with synaptophysin-SEP in terms of baseline fluorescence intensities and surface fractions (Figure 4D,E). In contrast to the results with TfR-Lime, synaptophysin-Lime does not exhibit higher brightness than synaptophysin-SEP. The reason for this difference is not known, but it may be related to the fact that Lime is inserted into a loop region of synaptophysin but fused to a terminus of TfR.

We next attempted to image neuronal membrane potential changes with Limeade (Lime A227D). We replaced SEP-D in the ArcLight-Q239 voltage sensor with Limeade to create a new voltage sensor termed ArcLimeade.[22] Expression of ArcLimeade in dissociated neurons resulted in well-defined membrane fluorescence (Figure 4F). Membrane depolarization (−70 to 30 mV) resulted in an ∼ 4% decrease in fluorescence intensity for both ArcLight and ArcLimeade (Figure 4G). In response to voltage steps changing from −70 to 50 mV in cultured neuron cells, ArcLimeade exhibited a total steady-state fluorescence change $\Delta F/F_0$ of −43 ± 1.6%, and ArcLight exhibited an identical change of −43 ± 0.8% (Figure 4H). ArcLimeade retained a sigmoidal fluorescence−voltage relationship with a $V_{1/2}$ at −32 mV, showing an overall similar voltage response compared to ArcLight-Q239 (Figure 4I). Altogether, these results established synaptophysin-Lime and ArcLimeade as sensitive indicators for the detection of membrane potential changes associated with neuronal activity.

CONCLUSIONS

Here, we have reported the rational engineering and characterization of improved SEP variants. Lime and its variants were designed based on the combination of cysteine-free superfolder GFP (oxGFP) and superecliptic pHluorin (SEP), with the goal of realizing enhanced properties. The resultant Lime variant is an improved pH-sensitive GFP with brighter molecular fluorescence and larger fluorescent intensity change over the physiological pH range.

We solved the atomic structure of Lime, which revealed an unexpected orientation rearrangement of residues 147 and 148, highlighting the flexibility of these two residues. With the identification of the key mutation S147D, we created pH-sensitive mutants of EGFP by only incorporating this single mutation, which is an effective approach to quickly create pH-sensitive GFP fusions from previously constructed EGFP or clover-based fusion constructs.

We demonstrated the use of the newly engineered SEP variants for imaging endocytosis, exocytosis, and neuronal activity. Relative to SEP, Lime exhibited significantly brighter fluorescence in the context of TfR fusions for endo- and exocytosis imaging. Synaptophysin-Lime and ArcLimeade also performed well in synaptic release and membrane voltage imaging, respectively. Overall, we believe that Lime and its variants are valuable additions to the toolbox of genetically encoded sensors.

MATERIAL AND METHODS

Protein Engineering and Molecular Biology. The DNA encoding Lime was synthesized by IDT. Rational engineering of Lime variants was performed via site-directed mutagenesis using plasmids encoding Lime as a template. Site-directed mutagenesis was performed using a QuikChange Lightning mutagenesis kit (Agilent Technologies) or a CloneAmp HiFi PCR premix (Takara Bio). Mutagenic primers were designed according to the QuikChange mutagenesis guidelines. A mutagenic product was used to transform the electrocompetent *Escherichia coli* (*E. coli*) strain DH10B (Thermo Scientific). Transformed *E. coli* were plated on agar plates containing LB medium supplemented with 0.4 mg/mL ampicillin and 0.02% wt/vol L-arabinose. Protein was extracted from overnight liquid culture using a B-PER bacterial extraction reagent (Thermo Scientific) as per the manufacturer's guidelines. Primary screening for pH sensitivity of extracted protein was performed with a Safire2 fluorescence plate reader (Tecan) by measuring protein fluorescence intensity in buffers with pH 5.5 and pH 7.5. Plasmid DNA was purified with a GeneJET

https://doi.org/10.1021/acssensors.3c00484
ACS Sens. XXXX, XXX, XXX−XXX

miniprep kit (Thermo Scientific) and then sequenced using a BigDye Terminator Cycle Sequencing kit (Applied Biosystems).

Protein Purification and *In Vitro* Characterization. To purify Lime and its variants, the electrocompetent *E. coli* strain DH10B was transformed using a Micropulser electroporator (Bio-Rad). Transformed bacteria were cultured overnight on agar plates containing LB and ampicillin. Single colonies were picked and grown overnight in 4 mL of LB supplemented with ampicillin at 37 °C. For each colony, the 4 mL culture was then used to inoculate 500 mL of LB medium with ampicillin and the addition of 0.02% arabinose and grown overnight at 37 °C. Bacteria were harvested by centrifugation and lysed by sonication. The protein was purified using Ni-NTA (G-biosciences) affinity chromatography. Extinction coefficients were measured by the alkali denaturation method. Fluorescence quantum yields were determined using EGFP as a standard.[40] Fluorescence intensity as a function of pH was determined by dispensing 2 μL of the protein solution into 50 μL of the desired pH buffer in triplicate into a 396-well clear-bottom plate (Thermo Scientific) and measured in a Safire2 plate reader. pH buffer solutions from pH 4 to 10 were prepared according to the Carmody buffer.[41]

Crystallization and Structure Determination. Size-exclusion chromatography-purified Lime protein fractions were pooled and concentrated to 16 mg/mL and used for crystallization trials. Initial crystallization was set up with 384-well plates via sitting drop vapor diffusion against commercially available kits at 20 °C. The Lime protein crystals were grown in multiple conditions and soaked in the buffer of 0.2 M lithium chloride, 0.1 M MES pH 6.0, 20% w/v PEG 6000, 0.2 M ammonium phosphate monobasic, 0.1 M Tris pH 10, and 50% v/v MPD. The crystals were cryoprotected with a reservoir supplemented with 20% glycerol in liquid nitrogen. X-ray diffraction data were collected at Beamline 08ID-1. The X-ray diffraction data were scaled using XDS,[42] and data collection statistics are summarized in Table S1. The Lime pH 10 and pH 6 datasets belonged to the trigonal space group $P3_121$ with one Lime molecule in the asymmetric unit. Molecular replacement was performed with Phaser using GFP protein as a search model.[43] The datasets of pH 10 and pH 6 were processed to 2.0 and 2.85 Å with similar unit cell parameters of a = 109 Å, b = 109 Å, and c = 49.9 Å. Model building and further refinement were carried out in Coot and Phenix.[44,45] The final model demonstrated R_{work}/R_{free} values of 0.1723/0.2056 and 0.2047/0.2534 for pH 10 and pH 6 datasets. All the refinement statistics are noted in Table S1.

Imaging Endocytosis and Exocytosis with TfR-Lime. The TfR-Lime construct was made by replacing SEP with Lime in the previously reported TfR-SEP construct.[37] BSC-1 cells (ECACC no. 85011422) were grown in DMEM supplemented with 10% fetal calf serum, 1% sodium pyruvate, and 1% Glutamax and maintained at 37 °C in 5% CO_2. Cells were passaged every 2−4 days for maintenance. Cells were transfected in T25 flasks with 1.5 μg of either TfR-SEP or TfR-LIMEDNA using a Fugene 6 (Promega) transfection reagent. Six hours post-transfection, cells were plated onto 18 mm glass coverslips precoated with 0.1 mg/mL poly-L-lysine and imaged 24 h post-transfection. Cells were perfused with HEPES-buffered saline (HBS) solution (135 mM NaCl, 5 mM KCl, 0.4 mM $MgCl_2$, 1.8 mM $CaCl_2$, 20 mM HEPES, and 1 mM D-glucose) at pH 7.4.

TIRF imaging was performed on an inverted microscope (IX71; Olympus) equipped with an Apochromat N oil 60× objective (NA 1.49), a 1.6× magnifying lens, and an EMCCD camera (QuantEM:512SC; Roper Scientific). Fluorescence emission was collected via a 525/50 filter (Chroma). Samples were illuminated by a 473 nm laser (Cobolt) for SEP and Lime imaging with identical laser intensity and camera settings. The ppH protocol for imaging endocytosis was performed as described previously[21] with a frame rate of 0.5 Hz (100 ms exposure time). Cycles of one image at pH 7.4, followed 2 s later by one image at pH 5.5, were repeated for at least 5 min. Imaging of exocytosis events was performed with continuous imaging at 10 Hz for 1 min.

To perform a Western blot, BSC-1 cells in 6-well plates were transfected with 0.5 μg plasmid/well encoding either TfR-SEP or TfR-Lime. Cells were lysed 30 h post-transfection in RIPA buffer supplemented with antiproteases, and 80 μg of each lysate was loaded and run on a 4−20% polyacrylamide gel. Proteins were transferred to a nitrocellulose membrane and blotted using anti-GFP (Roche ref. 11814460001) and antiactin (Sigma-Aldrich ref. A2066) primary antibodies.

Analysis of Endocytosis and Exocytosis Events with TfR-Lime. Detection and quantification of endocytosis events were conducted using custom-made Matlab (R2018b) scripts that have previously been described.[21] In short, a sudden, punctate, fluorescence increase appearing in pH 5.5 images was detected as being an endocytic event if (1) it was visible for more than 3 frames (i.e., 8 s) and (2) it appeared at the same location as a pre-existing fluorescence cluster detectable in pH 7.4 images. Candidate events from each cell were validated using a trained support vector machine as described previously.[21] The event frequency was expressed per cell surface area measured on the cell masks. The average fluorescence intensity was measured in a 4-pixel diameter circle (430 nm) minus a local background (annulus of 4-pixel inner diameter, 10-pixel outer diameter) centered on the detected vesicle (images at pH 5.5) until the vesicle disappears. Causes of vesicle disappearance include movement away from the cell surface and vesicle acidification. Figure 3F,G represents averages ± SEM of the fluorescence (at pH 7.4 and 5.5) aligned at the time of vesicle detection (time 0) of all detected events. Detection and quantification of exocytosis events were performed with custom-made Matlab (R2018b) scripts as described previously.[46] Exocytosis events were detected with an ad hoc threshold in a differential movie and further validated with automated and user-defined criteria. The event frequency was expressed per cell surface area measured on the cell masks. The average fluorescence in a 5-pixel diameter area (minus a local background) centered on the appearing vesicle was measured for each event. The decrease in fluorescence reflects diffusion of TfR in the plasma membrane after exocytosis.

Imaging Neuronal Exocytosis with Synaptophysin-Lime. All procedures followed the European legislation for animal experimentation (directive 2010/63/EU), and animal manipulations were approved by the institutional Ethical Committee. Wild-type rats were of the Sprague Dawley strain Crl:CD (SD), which are bred by Charles River Laboratories worldwide following the international genetic standard protocol (IGS). Hippocampal CA3-CA1 regions without dentate gyrus were isolated from 0- to 2-days-old rats of mixed gender, plated on poly-ornithine-coated coverslips, transfected 7 days after plating using calcium phosphate-mediated gene transfer, and imaged 14−21 days after plating as previously described.[47] These cultures resulted in mixed neuron-astrocyte cultures, which were maintained in culture media composed of MEM (Thermo Scientific), 0.5% glucose, 0.1 g/L bovine transferrin (Millipore Sigma), 0.25 g/L insulin (Millipore Sigma), 1% Glutamax (Thermo Scientific), 5−10% fetal bovine serum (Thermo Scientific), and 2% N-21 (Bio-Techne). Culture media was replaced 2−3 days later with culture media containing 2 μM cytosine β-D-arabinofuranoside (Millipore Sigma) to limit astrocyte overgrowth. Cultures were incubated at 37 °C in a 95% air/5% CO_2 humidified incubator for 14−21 days prior to use. Neuronal live-cell imaging was performed using a custom-built laser-illuminated epifluorescence microscope with an Andor iXon Ultra (model no. DU-897U-CSO-#BV) back-illuminated electron-multiplying charge-coupled device camera cooled to −90 °C. Experiments were performed at a clamped temperature of 36.5 °C using both an in-line solution heater (640104: SHM-6, multichannel systems) and a chamber heater platform (64-0285 PH-2, multichannel systems). Action potentials (AP) were evoked by passing 1 ms current pulses, yielding fields of approximately 7 V cm^{-1} via platinum-iridium electrodes using an imaging chamber that allows field stimulation (64-0226 RC-21BRFS, multichannel systems). Cells were continuously perfused at 0.1 mL/min with a Tyrode's solution containing (in mM) 119 NaCl, 2.5 KCl, 2 $CaCl_2$, 2 $MgCl_2$, and 30 glucose (Sigma-Aldrich G8270), 10 μM 6-cyano-7-nitroquinoxaline-2,3-dione (CNQX), and 50 μM D,L-2-amino-5-phosphonovaleric acid (AP5) to block postsynaptic AMPA and NMDA receptor responses, buffered to pH 7.4 using 25 mM HEPES. Synaptophysin-Lime was generated by

https://doi.org/10.1021/acssensors.3c00484
ACS Sens. XXXX, XXX, XXX−XXX

replacing SEP with Lime in synaptophysin-SEP. Synaptophysin-Lime-expressing neurons were imaged at 10 Hz, and responses to 10 AP at 10 Hz were recorded. Images were analyzed using the ImageJ plugin Time Series Analyzer V3, where typically 30−40 regions of interest (ROIs) corresponding to synaptic boutons were selected, and fluorescence was measured over time.

Imagining Neuronal Membrane Voltage with ArcLimeade. All procedures involving animals were conducted in accordance with protocols approved by the Howard Hughes Medical Institute Janelia Research Campus Institutional Animal Care and Use Committee and Institutional Biosafety Committee. Hippocampal neurons extracted from P0 to 1 Sprague Dawley rat pups were transfected with pcDNA3.1-CAG-ArcLimeade by electroporation (Lonza, P3 Primary Cell 4D-Nucleofector X kit). Neurons were plated onto 24-well glass-bottom plates (MaTek) coated with poly-D-lysine (Sigma). Neurons were cultured for 8−12 days in NbActiv4 medium (BrainBits). Imaging buffer (containing the following (in mM): 145 NaCl, 2.5 KCl, 10 glucose, 10 HEPES pH 7.4, 2 $CaCl_2$, and 1 $MgCl_2$) was used. Cultures were illuminated with a SPECTRA X light engine (Lumencor) and observed through a 40× oil objective (NA = 1.3, Nikon) on an inverted Nikon Eclipse Ti2 microscope. Excitation and emission light was passed through a FITC filter set (475/50 nm (excitation), 540/50 nm (emission), and a 506LP dichroic mirror (FITC-5050A-000; Semrock)) to image ArcLimeade. Fluorescence was collected by a CMOS camera (ORCA-Flash 4.0, Hamamatsu). A stimulus isolator (A385, World Precision Instruments) with platinum wires was used to deliver field stimuli to elicit action potentials in cultured neurons. For voltage-clamp experiments used to generate fluorescence−voltage curves, voltage steps (from −110 to +50 mV in 20 mV increments for 1 s) were applied to cells held at −70 mV. All recordings were done at room temperature.

■ ASSOCIATED CONTENT

Supporting Information

The Supporting Information is available free of charge at https://pubs.acs.org/doi/10.1021/acssensors.3c00484.

(Table S1) X-ray data collection and refinement statistics, (Figure S1) sequence alignment, (Figure S2) comparison of Lime structures at pH 10 and pH 6, and (Figure S3) comparison of TfR-SEP and TfR-Lime expression levels in BSC-1 cells (PDF)

■ AUTHOR INFORMATION

Corresponding Authors

Yi Shen − *Department of Chemistry, University of Alberta, Edmonton, Alberta T6G 2G2, Canada;* orcid.org/0000-0003-4117-0279; Email: yi.shen@ualberta.ca

Robert E. Campbell − *Department of Chemistry, University of Alberta, Edmonton, Alberta T6G 2G2, Canada; Department of Chemistry, Graduate School of Science, The University of Tokyo, Tokyo 113-0033, Japan;* orcid.org/0000-0003-0604-092X; Email: campbell@chem.s.u-tokyo.ac.jp

Authors

Yurong Wen − *Department of Biochemistry, Faculty of Medicine & Dentistry, University of Alberta, Edmonton, Alberta T6G 2H7, Canada; Center for Microbiome Research of Med-X Institute, The First Affiliated Hospital, Xi'an Jiaotong University, Xi'an, Shaanxi 710061, China*

Silvia Sposini − *CNRS, Interdisciplinary Institute for Neuroscience, UMR 5297, University of Bordeaux, Bordeaux 33076, France; Department of Metabolism, Digestion and Reproduction, Institute of Reproductive and Developmental Biology, Imperial College London, London SW7 2BX, United Kingdom*

Anjali Amrapali Vishwanath − *Institut du Cerveau-Paris Brain Institute-ICM, Inserm, CNRS, APHP, Häpital de la Pitié Salpêtrière, Sorbonne Université, 75013 Paris, France*

Ahmed S. Abdelfattah − *Janelia Research Campus, Howard Hughes Medical Institute, Ashburn, Virgina 20147, United States; Department of Neuroscience, Brown University, Providence, Rhode Island 02906, United States;* orcid.org/0000-0001-8131-1772

Eric R. Schreiter − *Janelia Research Campus, Howard Hughes Medical Institute, Ashburn, Virgina 20147, United States*

M. Joanne Lemieux − *Department of Biochemistry, Faculty of Medicine & Dentistry, University of Alberta, Edmonton, Alberta T6G 2H7, Canada;* orcid.org/0000-0003-4745-9153

Jaime de Juan-Sanz − *Institut du Cerveau-Paris Brain Institute-ICM, Inserm, CNRS, APHP, Häpital de la Pitié Salpêtrière, Sorbonne Université, 75013 Paris, France*

David Perrais − *CNRS, Interdisciplinary Institute for Neuroscience, UMR 5297, University of Bordeaux, Bordeaux 33076, France*

Complete contact information is available at: https://pubs.acs.org/10.1021/acssensors.3c00484

Author Contributions

Y.S. engineered Lime variants, assembled DNA constructs, performed protein characterization, analyzed data, prepared figures, and wrote the manuscript. Y.W. performed the protein crystallization, solved the structures, and analyzed data. S.S. performed imaging of TfR-Lime, analyzed data, and prepared figures. A.A.V. performed imaging of synaptophysin-Lime, analyzed data, and prepared figures. A.S.A. performed imaging of ArcLimeade, analyzed data, and prepared figures. E.R.S., M.J.L., J.d.J.-S., D.P., and R.E.C. supervised the research. All authors contributed to the editing and proofreading of the manuscript.

Notes

The authors declare no competing financial interest.

Plasmids and DNA sequences are available via Addgene. The Lime structures are deposited in the Protein Data Bank (PDB IDs 7YV3 and 7YV5). Data supporting the findings in this research are available from the corresponding author upon request.

■ ACKNOWLEDGMENTS

This work was supported by grants from the Canadian Institutes of Health Research (CIHR, FS-154310 to R.E.C.) and the Natural Sciences and Engineering Research Council of Canada (NSERC, RGPIN 2018-04364 to R.E.C. and RGPIN-2016-06478 to M.J.L.) and the Agence Nationale de la Recherche (LocalEndoProbes, ANR-17-CE16-0012, to D.P.). Y.W. was supported by the Alberta Parkinson Society Fellowship and the National Natural Science Foundation of China (nos. 31870132 and 82072237). S.S. was supported by a Sir Henry Wellcome Postdoctoral Fellowship (Wellcome Trust, 218650/Z/19/Z). Data were collected at beamline CMCF-ID at the Canadian Light Source, a national research facility of the University of Saskatchewan, which is supported by the Canada Foundation for Innovation (CFI), the NSERC, the National Research Council (NRC), the CIHR, the Government of Saskatchewan, and the University of Saskatchewan. A.S.A. and E.R.S. were supported by Howard Hughes Medical Institute. J.d.J.-S. and A.A.V. were supported

https://doi.org/10.1021/acssensors.3c00484
ACS Sens. XXXX, XXX, XXX−XXX

by the Paris Brain Institute Diane Barrière Chair in Synaptic Bioenergetics, an ERC Starting Grant SynaptoEnergy (852873), and the 2019 ATIP-Avenir program. J.d.J.-S. is a permanent CNRS researcher. Y.S. and R.E.C. thank the University of Alberta Molecular Biology Services Unit for technical assistance.

REFERENCES

(1) Greenwald, E. C.; Mehta, S.; Zhang, J. Genetically Encoded Fluorescent Biosensors Illuminate the Spatiotemporal Regulation of Signaling Networks. *Chem. Rev.* **2018**, *118*, 11707−11794.

(2) Nasu, Y.; Shen, Y.; Kramer, L.; Campbell, R. E. Structure- and Mechanism-Guided Design of Single Fluorescent Protein-Based Biosensors. *Nat. Chem. Biol.* **2021**, *17*, 509−518.

(3) Lin, M. Z.; Schnitzer, M. J. Genetically Encoded Indicators of Neuronal Activity. *Nat. Neurosci.* **2016**, *19*, 1142−1153.

(4) Shen, Y.; Nasu, Y.; Shkolnikov, I.; Kim, A.; Campbell, R. E. Engineering Genetically Encoded Fluorescent Indicators for Imaging of Neuronal Activity: Progress and Prospects. *Neurosci. Res.* **2020**, *152*, 3−14.

(5) Schweizer, F. E.; Ryan, T. A. The Synaptic Vesicle: Cycle of Exocytosis and Endocytosis. *Curr. Opin. Neurobiol.* **2006**, *16*, 298−304.

(6) Miesenböck, G.; De Angelis, D. A.; Rothman, J. E. Visualizing Secretion and Synaptic Transmission with PH-Sensitive Green Fluorescent Proteins. *Nature* **1998**, *394*, 192−195.

(7) Sankaranarayanan, S.; Ryan, T. A. Real-Time Measurements of Vesicle-SNARE Recycling in Synapses of the Central Nervous System. *Nat. Cell Biol.* **2000**, *2*, 197−204.

(8) Ashby, M. C.; Ibaraki, K.; Henley, J. M. It's Green Outside: Tracking Cell Surface Proteins with PH-Sensitive GFP. *Trends Neurosci.* **2004**, *27*, 257−261.

(9) Burrone, J.; Li, Z.; Murthy, V. N. Studying Vesicle Cycling in Presynaptic Terminals Using the Genetically Encoded Probe SynaptopHluorin. *Nat. Protoc.* **2006**, *1*, 2970−2978.

(10) Xu, J.; Chai, H.; Ehinger, K.; Egan, T. M.; Srinivasan, R.; Frick, M.; Khakh, B. S. Imaging P2X4 Receptor Subcellular Distribution, Trafficking, and Regulation Using P2X4-PHluorin. *J. Gen. Physiol.* **2014**, *144*, 81−104.

(11) Kavalali, E. T.; Jorgensen, E. M. Visualizing Presynaptic Function. *Nat. Neurosci.* **2014**, *17*, 10−16.

(12) Sankaranarayanan, S.; De Angelis, D.; Rothman, J. E.; Ryan, T. A. The Use of PHluorins for Optical Measurements of Presynaptic Activity. *Biophys. J.* **2000**, *79*, 2199−2208.

(13) Tantama, M.; Hung, Y. P.; Yellen, G. Imaging Intracellular PH in Live Cells with a Genetically Encoded Red Fluorescent Protein Sensor. *J. Am. Chem. Soc.* **2011**, *133*, 10034−10037.

(14) Li, Y.; Tsien, R. W. PHTomato, a Red, Genetically Encoded Indicator That Enables Multiplex Interrogation of Synaptic Activity. *Nat. Neurosci.* **2012**, *15*, 1047−1053.

(15) Shen, Y.; Rosendale, M.; Campbell, R. E.; Perrais, D. PHuji, a PH-Sensitive Red Fluorescent Protein for Imaging of Exo- and Endocytosis. *J. Cell Biol.* **2014**, *207*, 419−432.

(16) Liu, A.; Huang, X.; He, W.; Xue, F.; Yang, Y.; Liu, J.; Chen, L.; Yuan, L.; Xu, P. PHmScarlet Is a PH-Sensitive Red Fluorescent Protein to Monitor Exocytosis Docking and Fusion Steps. *Nat. Commun.* **2021**, *12*, 1−12.

(17) Raymond, M. H.; Davidson, A. J.; Shen, Y.; Tudor, D. R.; Lucas, C. D.; Morioka, S.; Perry, J. S. A.; Krapivkina, J.; Perrais, D.; Schumacher, L. J.; Campbell, R. E.; Wood, W.; Ravichandran, K. S. Live Cell Tracking of Macrophage Efferocytosis during *Drosophila* Embryo Development in Vivo. *Science* **2022**, *375*, 1182−1187.

(18) Jullie, D.; Choquet, D.; Perrais, D. Recycling Endosomes Undergo Rapid Closure of a Fusion Pore on Exocytosis in Neuronal Dendrites. *J. Neurosci.* **2014**, *34*, 11106−11118.

(19) Verweij, F. J.; Bebelman, M. P.; Jimenez, C. R.; Garcia-Vallejo, J. J.; Janssen, H.; Neefjes, J.; Knol, J. C.; de Goeij-de Haas, R.; Piersma, S. R.; Baglio, S. R.; Verhage, M.; Middeldorp, J. M.; Zomer, A.; van Rheenen, J.; Coppolino, M. G.; Hurbain, I.; Raposo, G.; Smit, M. J.; Toonen, R. F. G.; van Niel, G.; Pegtel, D. M. Quantifying Exosome Secretion from Single Cells Reveals a Modulatory Role for GPCR Signaling. *J. Cell Biol.* **2018**, *217*, 1129−1142.

(20) Taylor, M. J.; Perrais, D.; Merrifield, C. J. A High Precision Survey of the Molecular Dynamics of Mammalian Clathrin-Mediated Endocytosis. *PLoS Biol.* **2011**, *9*, No. e1000604.

(21) Sposini, S.; Rosendale, M.; Claverie, L.; Van, T. N. N.; Jullié, D.; Perrais, D. Imaging Endocytic Vesicle Formation at High Spatial and Temporal Resolutions with the Pulsed-PH Protocol. *Nat. Protoc.* **2020**, *15*, 3088−3104.

(22) Jin, L.; Han, Z.; Platisa, J.; Wooltorton, J. R. A.; Cohen, L. B.; Pieribone, V. A. Single Action Potentials and Subthreshold Electrical Events Imaged in Neurons with a Fluorescent Protein Voltage Probe. *Neuron* **2012**, *75*, 779−785.

(23) Ashby, M. C.; De La Rue, S. A.; Ralph, G. S.; Uney, J.; Collingridge, G. L.; Henley, J. M. Removal of AMPA Receptors (AMPARs) from Synapses Is Preceded by Transient Endocytosis of Extrasynaptic AMPARs. *J. Neurosci.* **2004**, *24*, 5172−5176.

(24) Rathje, M.; Fang, H.; Bachman, J. L.; Anggono, V.; Gether, U.; Huganir, R. L.; Madsen, K. L. AMPA Receptor PHluorin-GluA2 Reports NMDA Receptor-Induced Intracellular Acidification in Hippocampal Neurons. *Proc. Natl. Acad. Sci. U. S. A.* **2013**, *110*, 14426−14431.

(25) Ventimiglia, D.; Bargmann, C. I. Diverse Modes of Synaptic Signaling, Regulation, and Plasticity Distinguish Two Classes of C. Elegans Glutamatergic Neurons. *Elife* **2017**, *6*, No. e31234.

(26) Cabantous, S.; Waldo, G. S. In Vivo and in Vitro Protein Solubility Assays Using Split GFP. *Nat. Methods* **2006**, *3*, 845−854.

(27) Costantini, L. M.; Baloban, M.; Markwardt, M. L.; Rizzo, M. A.; Guo, F.; Verkhusha, V. V.; Snapp, E. L. A Palette of Fluorescent Proteins Optimized for Diverse Cellular Environments. *Nat. Commun.* **2015**, *6*, 7670.

(28) Costantini, L. M.; Fossati, M.; Francolini, M.; Snapp, E. L. Assessing the Tendency of Fluorescent Proteins to Oligomerize under Physiologic Conditions. *Traffic* **2012**, *13*, 643−649.

(29) Zacharias, D. A.; Violin, J. D.; Newton, A. C.; Tsien, R. Y. Partitioning of Lipid-Modified Monomeric GFPs into Membrane Microdomains of Live Cells. *Science* **2002**, *296*, 913−916.

(30) Han, Z.; Jin, L.; Chen, F.; Loturco, J. J.; Cohen, L. B.; Bondar, A.; Lazar, J.; Pieribone, V. A. Mechanistic Studies of the Genetically Encoded Fluorescent Protein Voltage Probe ArcLight. *PLoS One* **2014**, *9*, No. e113873.

(31) Ormö, M.; Cubitt, A. B.; Kallio, K.; Gross, L. A.; Tsien, R. Y.; Remington, S. J. Crystal Structure of the Aequorea Victoria Green Fluorescent Protein. *Science* **1996**, *273*, 1392−1395.

(32) Shu, X.; Kallio, K.; Shi, X.; Abbyad, P.; Kanchanawong, P.; Childs, W.; Boxer, S. G.; Remington, S. J. Ultrafast Excited-State Dynamics in the Green Fluorescent Protein Variant S65T/H148D. 1. Mutagenesis and Structural Studies. *Biochemistry* **2007**, *46*, 12005−12013.

(33) Hanson, G. T.; McAnaney, T. B.; Park, E. S.; Rendell, M. E. P.; Yarbrough, D. K.; Chu, S.; Xi, L.; Boxer, S. G.; Montrose, M. H.; Remington, S. J. Green Fluorescent Protein Variants as Ratiometric Dual Emission PH Sensors. 1. Structural Characterization and Preliminary Application. *Biochemistry* **2002**, *41*, 15477−15488.

(34) Heim, R.; Cubitt, A. B.; Tsien, R. Y. Improved Green Fluorescence. *Nature* **1995**, *373*, 663−664.

(35) Bajar, B. T.; Wang, E. S.; Lam, A. J.; Kim, B. B.; Jacobs, C. L.; Howe, E. S.; Davidson, M. W.; Lin, M. Z.; Chu, J. Improving Brightness and Photostability of Green and Red Fluorescent Proteins for Live Cell Imaging and FRET Reporting. *Sci. Rep.* **2016**, *6*, 20889.

(36) Ong, W. S. Y.; Ji, K.; Pathiranage, V.; Maydew, C.; Baek, K.; Villones, R. L. E.; Meloni, G.; Walker, A. R.; Dodani, S. C. Rational Design of the B-bulge Gate in a Green Fluorescent Protein Accelerates the Kinetics of Sulfate Sensing. *Angew. Chem.* **2023**, No. e202302304.

https://doi.org/10.1021/acssensors.3c00484
ACS Sens. XXXX, XXX, XXX−XXX

(37) Merrifield, C. J.; Perrais, D.; Zenisek, D. Coupling between Clathrin-Coated-Pit Invagination, Cortactin Recruitment, and Membrane Scission Observed in Live Cells. *Cell* **2005**, *121*, 593−606.
(38) Xu, Y.; Rubin, B. R.; Orme, C. M.; Karpikov, A.; Yu, C.; Bogan, J. S.; Toomre, D. K. Dual-Mode of Insulin Action Controls GLUT4 Vesicle Exocytosis. *J. Cell Biol.* **2011**, *193*, 643−653.
(39) Zhu, Y.; Xu, J.; Heinemann, S. F. Two Pathways of Synaptic Vesicle Retrieval Revealed by Single-Vesicle Imaging. *Neuron* **2009**, *61*, 397−411.
(40) Cranfill, P. J.; Sell, B. R.; Baird, M. A.; Allen, J. R.; Lavagnino, Z.; de Gruiter, H. M.; Kremers, G.-J.; Davidson, M. W.; Ustione, A.; Piston, D. W. Quantitative Assessment of Fluorescent Proteins. *Nat. Methods* **2016**, *13*, 557−562.
(41) Carmody, W. R. Easily Prepared Wide Range Buffer Series. *J. Chem. Educ.* **1961**, *38*, 559.
(42) Kabsch, W. XDS. *Acta Crystallogr., Sect. D: Biol. Crystallogr.* **2010**, *66*, 125−132.
(43) McCoy, A. J. Solving Structures of Protein Complexes by Molecular Replacement with Phaser. *Acta Crystallogr., Sect. D: Biol. Crystallogr.* **2007**, *63*, 32−41.
(44) Emsley, P.; Lohkamp, B.; Scott, W. G.; Cowtan, K. Features and Development of Coot. *Acta Crystallogr., Sect. D: Biol. Crystallogr.* **2010**, *66*, 486−501.
(45) Adams, P. D.; Afonine, P. V.; Bunkóczi, G.; Chen, V. B.; Davis, I. W.; Echols, N.; Headd, J. J.; Hung, L.-W.; Kapral, G. J.; Grosse-Kunstleve, R. W.; McCoy, A. J.; Moriarty, N. W.; Oeffner, R.; Read, R. J.; Richardson, D. C.; Richardson, J. S.; Terwilliger, T. C.; Zwart, P. H. PHENIX: A Comprehensive Python-Based System for Macromolecular Structure Solution. *Acta Crystallogr., Sect. D: Biol. Crystallogr.* **2010**, *66*, 213−221.
(46) Bakr, M.; Jullié, D.; Krapivkina, J.; Paget-Blanc, V.; Bouit, L.; Petersen, J. D.; Retailleau, N.; Breillat, C.; Herzog, E.; Choquet, D.; Perrais, D. The VSNAREs VAMP2 and VAMP4 Control Recycling and Intracellular Sorting of Post-Synaptic Receptors in Neuronal Dendrites. *Cell Rep.* **2021**, *36*, No. 109678.
(47) de Juan-Sanz, J.; Holt, G. T.; Schreiter, E. R.; de Juan, F.; Kim, D. S.; Ryan, T. A. Axonal Endoplasmic Reticulum Ca2+ Content Controls Release Probability in CNS Nerve Terminals. *Neuron* **2017**, *93*, 867−881.e6.

https://doi.org/10.1021/acssensors.3c00484
ACS Sens. XXXX, XXX, XXX−XXX